

Effect of polarisation on two-photon resonance in a large Zeeman manifold

Nayan Sharma, Ranjit Kumar Singh, and Ajay Tripathi

Department of Physics, Sikkim University, 6th Mile Samdur, East Sikkim, India -737102

Souvik Chatterjee

*Department of Chemistry, Amity Institute of Applied Sciences,
Amity University, Sector-125, Noida, Uttar Pradesh 201313, India.*

Prasanta K. Panigrahi

*Department of Physical Sciences, Indian Institute of Science Education
and Research Kolkata, Mohanpur 741246, West Bengal, India.*

In this study, we present numerical investigations on a large Zeeman manifold in an electromagnetically induced transparency (EIT) medium, focusing on the D_1 and D_2 lines of ^{87}Rb as our model system. We examine two distinct models comprising 13 and 16 energy levels, respectively, using pump-probe spectroscopy with varying polarization of the light fields. A longitudinal magnetic field is used, and the ellipticity of both light fields is varied with the constraint that both lights have orthogonal polarization. We discover that in the presence of a longitudinal magnetic field, the change in ellipticity of light polarization induces optical anisotropy. This anisotropy results from the uneven distribution of population among the ground Zeeman levels, leading to the absorption of weak probe light. For a large number of states interacting with different field components, the existence of a steady state depends upon the multi-photon resonance and phase matching conditions. A comment is made on why such conditions are not required in our model, and the assumptions and limitations of the model are also discussed. To validate our numerical findings, we perform experimental measurements at two different magnetic field strengths in the D_2 line of ^{87}Rb . The experimental results align well with our numerical simulations. Specifically, we conclude that the probe transmission spectra at lower magnetic field values (up to 20 G) exhibit similarity for both the D_1 and D_2 lines of ^{87}Rb , effectively described by the 13-level model. However, at higher magnetic field values, a more complicated 16-level (or higher) system is necessary to accurately capture the response of the probe in D_2 line.

I. INTRODUCTION

The interaction of light fields with multi-level atoms gives rise to various non-linear optical phenomena. These are often multi-photon processes that are based on quantum interference between the various excitation pathways [1]. The phenomena of electromagnetically induced transparency (EIT) [2–4], electromagnetically induced absorption (EIA) [5, 6], coherent population trapping (CPT) [7, 8], four wave mixing (FWM) [9, 10], six wave mixing [11–13], two-photon absorption (TPA) [14, 15] and others are some examples where multi-photon processes are dominant. These phenomena are extensively studied using hyperfine levels of alkali metals like Rb, Cs, Na, e.t.c., in an atomic vapor system [16–20]. Atomic vapor systems in the presence of a magnetic field are an excellent platform to study the interaction of light fields with multi-level atoms. Moreover, since the atomic medium is quantum mechanical in nature, the magnetic field (B) provides a preferred axis for the measurement of the observables of the system. In experiments, the resonances are observed either by changing the frequency detuning of one of the light field or by using a time dependent magnetic field (Hanle configuration). Without magnetic fields, it has been shown that the nature of the resonance can be controlled by adding the field components [21, 22] and by changing

the phase as well as the polarization state of the light field in systems such as Λ , N and tripod types [23–25]. On the other hand, in Hanle configuration, the effect of the ellipticity in the light polarisation is known to have a significant effect on the EIT/EIA resonances. By changing the polarisation states the amplitude of the EIT/EIA resonances can be controlled [26]. Also, change in ellipticity can result in conversion of EIT to EIA (vice-versa) as mentioned in [27–29].

In presence of a static magnetic field, two-photon resonances can switch between transmission and absorption at room temperature in both D_1 and D_2 line of ^{87}Rb [30, 31]. Using two light fields of linear orthogonal polarisation ($\text{lin}\perp\text{lin}$), the number of two-photon resonances in the probe spectra can be changed by using a different direction of the magnetic field [32]. By changing the direction of the magnetic field, the polarisations of the light fields are redefined, modifying the number of Λ systems that are responsible for such change in the number of resonances. Detailed study of the nature of EIT resonances in atomic vapor systems at both low and high magnetic field values has been performed by various groups [33–39].

However, a thorough literature review indicates that there is a lack of detailed investigation on the effects of light polarisation on two-photon resonances in presence

of a fixed static magnetic field (non-Hanle configuration) in EIT medium. In the present work we attempt to fill this research gap by investigating the effects of light polarisation, for a multi level atomic EIT system, interacting with two light fields (pump and probe) in presence of a magnetic field. The model case is briefly discussed below.

Model Case: D₁ and D₂ line of ⁸⁷Rb

We take a case where a Λ system is formed with two light fields (weak probe and strong pump) using the hyperfine levels $|F' = 1\rangle$, $|F' = 2\rangle$ and $|F' = 2\rangle$ for both D₁ and D₂ line of ⁸⁷Rb as shown in Fig.1.(a). and (b). At room temperature (300 K) the Doppler width (FWHM) of ⁸⁷Rb is 511 MHz. For D₁ line, the nearest excited state is $|F' = 1\rangle$ with a frequency gap of 817 MHz which is larger than the Doppler width. On the other hand, for D₂ line the frequency gap between $|F' = 2\rangle$ and $|F' = 1\rangle$ is 157 MHz which is well within the Doppler width. Hence, the effect of the nearby state $|F' = 1\rangle$ (if any) would be more pronounced in case of D₂ line for our model. Therefore, we study two different systems having 3 and 4 hyperfine levels for D₁ and D₂ lines respectively. In absence of magnetic field, the model system comprises of 13 and 16 degenerate energy levels for D1 and D2 lines respectively. After the application of the magnetic field all of these levels become nondegenerate. We consider a case where the polarisation of both the light fields are orthogonal to each other. The quantization axis is fixed by the direction of the static magnetic field which is along the propagation direction (longitudinal magnetic field). Hence, if both the fields are linearly polarized (lin \perp lin) the atomic frame would measure the light as equal mix of σ^+ and σ^- light. The energy level diagram for this case with the Zeeman levels (without splitting) is shown in Fig.1 (a) and (b).

Typically for numerical calculations different Λ systems are identified and treated as individual systems. The final spectra is then reproduced by summing up the contributions of all the individual Λ systems. This approach however fails to reproduce the experimental spectra even at moderate value of magnetic field where simultaneous presence of two photon absorption and EIT are present at different frequencies. On the other hand, for models with large number of energy states, the existence of steady state depends on the existence of time and phase independent basis for the system. We present a simple derivation to show that just by counting the number of field components and available energy states the existence of such basis can be commented upon. Rest of the article is organised as follows, first we introduce the equations in section II, followed by a detailed discussion of results for 13 level and 16 level systems in section III. In section IV we present a comment on the existence of steady state solutions followed by a discussion on the assumptions and limitations of our model in IV A. We

also present an experiment performed in D₂ line of ⁸⁷Rb which are in agreement with the numerical results in section V. Finally, the article is concluded in section VI where possible applications of our work is also discussed.

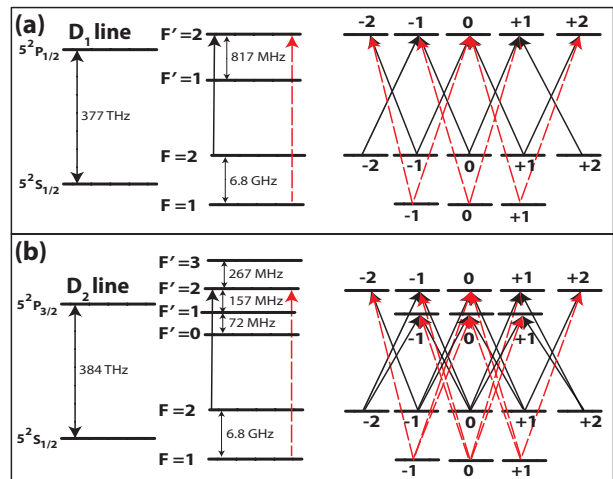


FIG. 1. Model system: (a) D₁ line with degenerate Zeeman levels making it a 13-level system and (b) D₂ line which is treated as a 16-level system. A weak probe (red and dashed) locked in $|F = 1\rangle \rightarrow |F' = 2\rangle$ transition and strong pump (Black and solid) scanning around $|F = 2\rangle \rightarrow |F' = 2\rangle$ transition is used to form a Λ system in absence of magnetic field.

II. EQUATIONS

We consider the light fields to be plane waves with elliptical polarisation,

$$\vec{E} = \vec{E}_p(e^{i\omega_p t} + e^{-i\omega_p t}) + \vec{E}_c(e^{i\omega_c t} + e^{-i\omega_c t}) \quad (1)$$

where, ω_p and ω_c are the frequency of the probe and pump respectively. The spatial dependence of the phase ($e^{\pm ikz}$) part is neglected using the Dipole approximation. The vector amplitudes which includes polarisation are,

$$\vec{E}_p = E_p \hat{e}_p, \quad \vec{E}_c = E_c \hat{e}_c \quad (2)$$

Where, \hat{e}_p and \hat{e}_c are represented in circular basis in the following manner,

$$\hat{e}_p = +\sin(\epsilon - \frac{\pi}{4}) \hat{e}_+ - \cos(\epsilon - \frac{\pi}{4}) \hat{e}_- \quad (3)$$

$$\hat{e}_c = -\cos(\epsilon - \frac{\pi}{4}) \hat{e}_+ - \sin(\epsilon - \frac{\pi}{4}) \hat{e}_- \quad (4)$$

Where, ϵ is the ellipticity and $\hat{e}_{\pm} = \mp(\frac{\hat{e}_x \pm i\hat{e}_y}{\sqrt{2}})$ are the circular basis. Note that the constraint $\hat{e}_p \cdot \hat{e}_c = 0$ allows us to define only one ellipticity parameter ϵ to represent the

polarisation state of both the light fields (Fig.2). Ellipticity is defined within the range $-\frac{\pi}{4} \leq \epsilon \leq \frac{\pi}{4}$, for which $\epsilon = 0$ represents linearly polarised states and $\epsilon = \pm \frac{\pi}{4}$ represents circular polarisations. The fields in the new basis are,

$$\vec{E}_p = E_p^+ \hat{e}_+ + E_p^- \hat{e}_-, \quad \vec{E}_c = E_c^+ \hat{e}_+ + E_c^- \hat{e}_- \quad (5)$$

where, $E_p^+ = E_p \sin(\epsilon - \frac{\pi}{4})$ and so on. The total Hamiltonian for the system is defined as,

$$H = H_0 + H_I + H_B \quad (6)$$

H_0 and H_I represents bare state and interaction Hamiltonian respectively. H_B represents the energy corrections due to the magnetic field. For a 16 level system using the rotating wave approximation (RWA) we have,

$$H_0 = \hbar(\delta_p - \delta_c) \sum_{i=4}^8 |i\rangle \langle i| + \hbar(\delta_p - \Delta - kv) \sum_{i=9}^{11} |i\rangle \langle i| + \hbar(\delta_p - kv) \sum_{i=12}^{16} |i\rangle \langle i| \quad (7)$$

Where, δ_p and δ_c are the frequency detuning of the probe and pump from the transitions $|F=1\rangle \rightarrow |F'=2\rangle$ and $|F=2\rangle \rightarrow |F'=2\rangle$ respectively. Δ is the frequency gap between the excited hyperfine states ($|F'=2\rangle$ and $|F'=1\rangle$).

$$H_I = -\frac{\hbar}{2} [\Omega_p^+ (c_{1,10} |1\rangle \langle 10| + c_{1,14} |1\rangle \langle 14| + c_{2,11} |2\rangle \langle 11| + c_{2,15} |2\rangle \langle 15| + c_{3,16} |3\rangle \langle 16| + \Omega_p^- (c_{1,12} |1\rangle \langle 12| + c_{2,9} |2\rangle \langle 9| + c_{2,13} |2\rangle \langle 13| + c_{3,10} |3\rangle \langle 10| + c_{3,14} |3\rangle \langle 14|) + \Omega_c^+ (c_{4,9} |4\rangle \langle 9| + c_{4,13} |4\rangle \langle 13| + c_{5,10} |5\rangle \langle 10| + c_{5,14} |5\rangle \langle 14| + c_{6,15} |6\rangle \langle 15| + c_{6,11} |6\rangle \langle 11| + c_{7,16} |7\rangle \langle 16|) + \Omega_c^- (c_{5,12} |5\rangle \langle 12| + c_{6,9} |6\rangle \langle 9| + c_{6,13} |6\rangle \langle 13| + c_{7,10} |7\rangle \langle 10| + c_{7,14} |7\rangle \langle 14| + c_{8,11} |8\rangle \langle 11| + c_{8,15} |7\rangle \langle 16|)] + h.c.$$

Ω_p^\pm and Ω_c^\pm are the reduced Rabi frequencies defined as,

$$\Omega_p^\pm = \frac{E_p^\pm \langle J || e\mathbf{r} || J' \rangle}{\hbar} \quad \Omega_c^\pm = \frac{E_c^\pm \langle J || e\mathbf{r} || J' \rangle}{\hbar} \quad (8)$$

$c_{i,j}$ is the Clebsch-Gordan coefficient which defines the transition strengths between the Zeeman levels [40].

$$H_B = \mu_B B \sum_{i=1}^{16} m_{F_i} g_{F_i} |i\rangle \langle i| \quad (9)$$

Where, m_{F_i} and g_{F_i} are the magnetic quantum number and Lande' g factor associated with the state $|i\rangle$ respectively. μ_B is the Bohr magneton and B is the strength

of the magnetic field. Similarly, the Hamiltonian for a 13 level system can also be written. Time evolution of the system within Density matrix formulation is given by,

$$\dot{\rho}(\delta_c, v) = -\frac{i}{\hbar} [H(\delta_c, v), \rho(\delta_c, v)] - \frac{1}{2} \{ \Gamma, \rho(\delta_c, v) \} - \gamma \rho(\delta_c, v) \quad (10)$$

Γ (of the order of MHz) is the relaxation matrix which

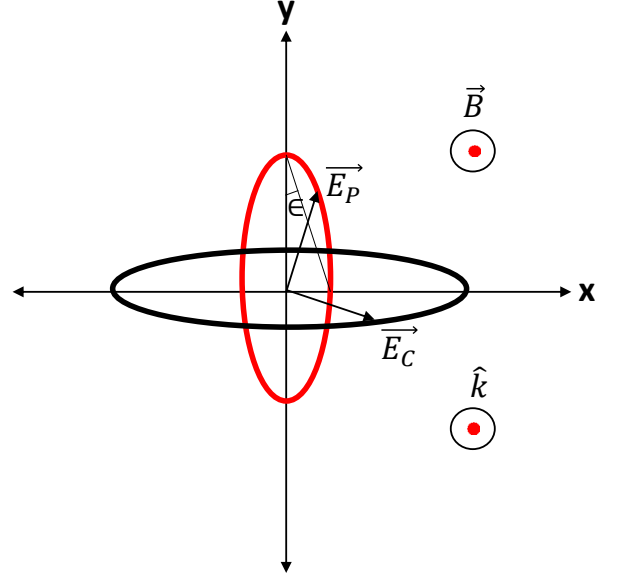


FIG. 2. The ellipticity vectors of probe (red) and pump (black) along with the direction of magnetic field (\vec{B}) and light propagation vector (\hat{k}).

incorporates the spontaneous decays out of the excited state. γ is the decay rate due to collisions of atoms which is typically of the order of few KHz at room temperature. The velocity distribution function of the atoms as a function of temperature is given by,

$$f(v) = \sqrt{\frac{m}{2\pi K_B T}} \exp(-\frac{mv^2}{2K_B T}) \quad (11)$$

Equation 10 is solved under the steady state condition $\dot{\rho} = 0$ to find the density matrix elements at every particular velocity in the range -300 m/s to 300 m/s. These density matrix elements are then averaged using $f(v)$ as a kernel to get the final results,

$$\bar{\rho}_{i,j}(\delta_c) = \int dv f(v) \rho(\delta_c, v) \quad (12)$$

III. RESULTS AND DISCUSSION

A. 13 level system

For a 13-level system, the response of the probe field is found by calculating the susceptibility given by,

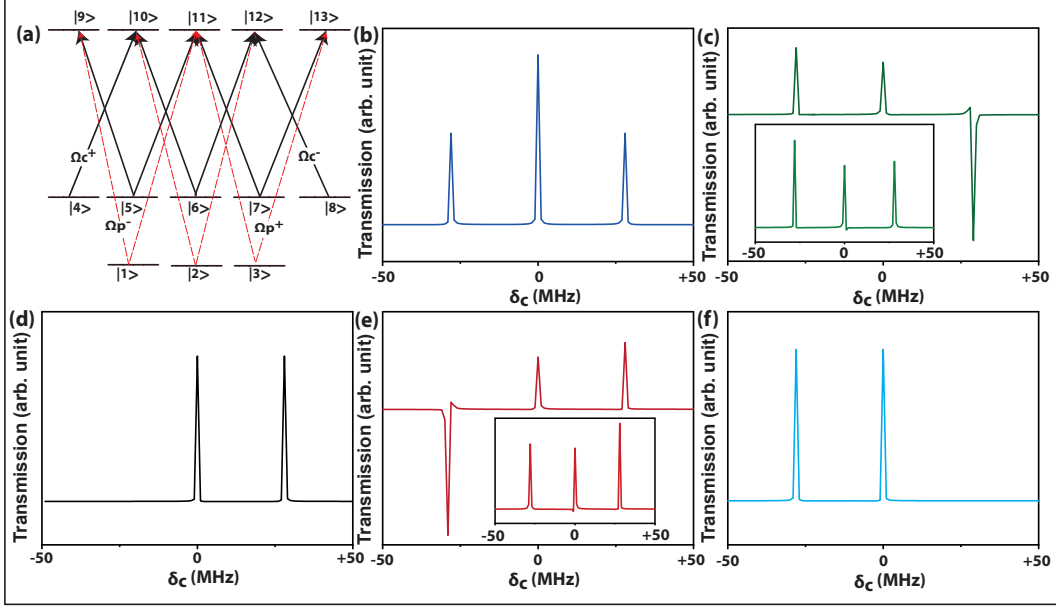


FIG. 3. (a) The energy level diagram showing 13 levels taken as zeeman sublevels (without the splitting). The red (dashed) line represents the weak probe and the black (solid) line is used to represent the strong probe. Numerical results showing transmission of the weak probe as a function of pump detuning (δ_c) at fixed value of $B=20\text{G}$, probe intensity = 0.3 mW/cm^2 and pump intensity = 161.2 mW/cm^2 : (b). three transmission peaks for ellipticity ($\epsilon=0^0$), (c). two transmission and one absorption (at blue detuned part) for $\epsilon = +30^0$. Inset shows that three transmission is possible if the coherence term $\bar{\rho}_{1,11}$ is excluded from the calculations (Eq.13), (d). two transmission peaks for $\epsilon = +45^0$, (e). two transmission and one absorption (at red detuned part) for $\epsilon = -30^0$. Inset shows that three transmission in this case is possible if the coherence term $\bar{\rho}_{3,11}$ is excluded from the calculations (Eq.13) and (f). two transmission peaks for $\epsilon = -45^0$.

$$\chi_p(\delta_c) = \frac{2N|d|^2}{\hbar\epsilon_0} [(\Omega_p^+)^{-1}(c_{1,11}\bar{\rho}_{1,11} + c_{2,12}\bar{\rho}_{2,12} + c_{3,13}\bar{\rho}_{3,13}) + (\Omega_p^-)^{-1}(c_{1,9}\bar{\rho}_{1,9} + c_{2,10}\bar{\rho}_{2,10} + c_{3,11}\bar{\rho}_{3,11})] \quad (13)$$

Where, N is the number density and ϵ_0 is the permittivity of free space and $d = \langle J | |er| | J' \rangle$. Finally, the transmission of the probe is calculated using the imaginary part of the susceptibility,

$$T = T_0 e^{-k|\text{Im}(\chi_p)|L} \quad (14)$$

Where, L is the length of the cell containing the atomic vapor. The numerical transmission spectra are shown in Fig.3. The calculations are performed for five different values of ellipticity ($\epsilon = 0, \pm\pi/6, \pm\pi/4$) with a fixed magnetic field of $B=20\text{ G}$. The energy level diagram without Zeeman splitting for this case is shown in Fig.3.(a). The probe and pump intensity are kept fixed at 0.3 mW/cm^2 and 161.2 mW/cm^2 respectively, throughout the evaluations. Figure 3 (b) shows the spectra for $\epsilon = 0$ in which both the σ^\pm components of the pump and probe have equal intensity. Three different transmission peaks are observed in this case, each of which is the superposition of different two-photon resonances due to a Λ system. There are in total ten Λ

systems present in this case whose two-photon resonance condition is satisfied at $\delta_c = 0 \pm 2\Delta_g$ ($\Delta_g = \frac{\mu_B B}{2\hbar}$). Out of the ten Λ , four are responsible for the transmission at $\delta_c = 0$. For each transmission at $\delta_c = \pm 2\Delta_g$ there is a superposition of three such Λ systems. The amplitude of the transmission at $\delta_c = 0$ is larger as compared to the one at $\delta_c = \pm\Delta_g$ due to the involvement of a larger number of Λ systems (hence a larger population).

Figure 3.(c). shows the result for the case of $\epsilon = \frac{\pi}{6}$, where it was observed that the two photon resonance at $\delta_c = 2\Delta_g$ i.e, the blue detuned peak flips and converts to an absorption. Also, the amplitude of the transmission at $\delta_c = 0$ is smaller as compared to the $\epsilon = 0$ case. This suggests that the large populations in the system are now undergoing two-photon absorption. It was found that if we calculate the susceptibility Eq.14 without the coherence term $\bar{\rho}_{1,11}$ the transmission is recovered in the spectra, which is shown in the inset of Fig. 3 (c). For this value of ellipticity, we have $\Omega_c^+ > \Omega_c^-$ ($\Omega_p^+ < \Omega_p^-$) which leads to population accumulation at the state $|8\rangle$ ($|F=2, m_F=+2\rangle$). This occurs because the transition $|8\rangle \rightarrow |12\rangle$ has a low value of rabi-frequency ($c_{8,12}\Omega_c^-$). Such unequal population distribution creates optical anisotropy in the medium where a weak σ^+ probe component ($\bar{\rho}_{1,11}$) gets absorbed near the two-photon resonance condition

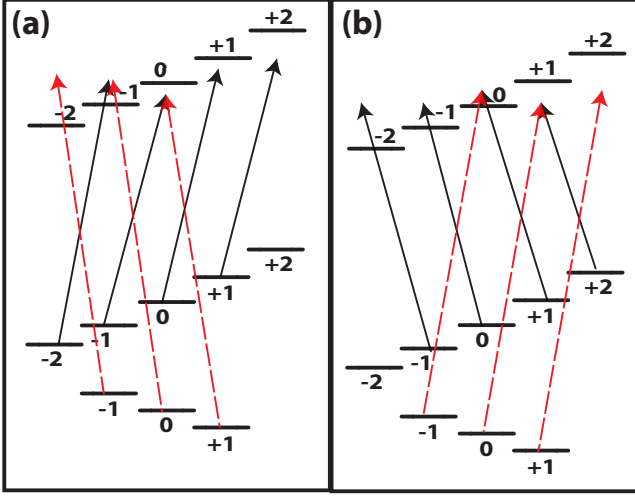


FIG. 4. Energy level diagrams for 13-level system showing the formation of two Λ systems each in case of (a). $\epsilon = +45^\circ$ and (b). $\epsilon = -45^\circ$

with a small light shift, which is of the order of $(\Omega_c^+)^2/\delta_p$.

The result for $\epsilon = \frac{\pi}{4}$ (pump is σ^- and probe is σ^+) is shown in Fig. 3 (d). For this case, we find that there are two transmission peaks at $\delta_c = 0$ and $\delta_c = 2\Delta_g$ and the resonance at $\delta_c = -2\Delta_g$ is missing. The reason for the observation is simple, as for this polarisation there are only two Λ systems present (Fig.4.(a)). Also, the weak σ^+ component of the probe undergoing absorption at $\epsilon = \frac{\pi}{6}$ is absent in this case.

For the cases of $\epsilon = -\frac{\pi}{6}$ and $\epsilon = -\frac{\pi}{4}$ the results are shown in Fig.3 (e) and (f), respectively. The observations are symmetric with respect to the ones obtained for $\epsilon = \frac{\pi}{6}$ and $\epsilon = \frac{\pi}{4}$. Figure 3 (e) shows the result for which the condition $\Omega_c^- > \Omega_c^+$ ($\Omega_p^- < \Omega_p^+$) is maintained, i.e., $\epsilon = -\frac{\pi}{6}$. We find that the absorption for this case occurs at the red detuning part ($\delta_c = -2\Delta_g$) which is related to the coherence term $\bar{\rho}_{3,11}$. Like in the previous case, the spectra without the term $\bar{\rho}_{3,11}$ had no absorption, as shown in the inset of Fig.3.(e). Hence, a weak σ^- component of the probe undergoes absorption in the presence of a relatively stronger σ^+ at near two-photon resonance. Finally, the result for $\epsilon = -\frac{\pi}{4}$ (Fig.3.(f)) reveals two transmission peaks at $\delta_c = 0$ and $\delta_c = -2\Delta_g$ which are due to the two Λ system formed by the σ^- pump and σ^+ probe as seen from the energy level diagram shown in Fig.4.(b).

B. 16 level system

The numerical calculations for the 16-level system are performed at 30 G. The reason for choosing a larger magnetic field is to involve the Zeeman states of the other

excited state. The energy levels diagram with the Zeeman states is shown in Fig.5.(a). The susceptibility of the probe field in this case is calculated as follows:

$$\chi_p(\delta_c) = \frac{2N|d|^2}{\hbar\epsilon_0} [(\Omega_p^+)^{-1}(c_{1,10} \bar{\rho}_{1,10} + c_{1,14} \bar{\rho}_{1,14} + c_{2,11} \bar{\rho}_{2,11} + c_{2,15} \bar{\rho}_{2,15} + c_{3,16} \bar{\rho}_{3,16}) + (\Omega_p^-)^{-1}(c_{1,12} \bar{\rho}_{1,12} + c_{2,9} \bar{\rho}_{2,9} + c_{2,13} \bar{\rho}_{2,13} + c_{3,10} \bar{\rho}_{3,10} + c_{3,14} \bar{\rho}_{3,14})] \quad (15)$$

The numerical transmission (Eq.14) spectra for this case are shown in Fig.5. For $\epsilon = 0$ i.e., for linearly polarised light fields, three transmission peaks are observed at $\delta_c = 0, \pm 2\Delta_g$. For 16-level system, we find there are in total 18 Λ systems out of which five each are responsible for transmission at $\delta_c = \pm 2\Delta_g$ and the remaining eight superpose at $\delta_c = 0$. The amplitude of the transmission peak at $\delta_c = -2\Delta_g$ is larger than the other two. The reason for this is that the inclusion of extra Zeeman levels changes the population distribution through optical pumping in such a way that larger populations are accumulated at $|3\rangle$.

For $\epsilon = \frac{\pi}{6}$ i.e., when $\Omega_c^+ > \Omega_c^-$ ($\Omega_p^+ < \Omega_p^-$), similar to the 13-level system, the transmission at $\delta_c = +2\Delta_g$ converts to an absorption dip. Unlike the 13-level system, the transmission at $\delta_c = 0$ shows some asymmetric line shape in this case. Such asymmetry arises due to the coupling of light fields with the Zeeman levels of the nearby excited state [41]. We calculated the susceptibility (Eq.15) without the coherence terms $\bar{\rho}_{1,10}$ and $\bar{\rho}_{1,14}$ and got the transmission back in the spectra as shown in the inset of Fig.5.(c). Hence, in this case also, a weak σ^+ component of the probe is absorbed in the presence of a strong σ^- component (and a strong σ^+ of the pump).

Next, the calculations are performed at $\epsilon = +\frac{\pi}{4}$ for which the result is shown in Fig.5.(d). The results are similar to those of the 13-level system, where we find two transmission peaks at $\delta_c = 0$ and $\delta_c = 2\Delta_g$. For this case where the light fields are circularly polarised (σ^- probe and σ^+ pump) two Λ systems superpose to give transmission peaks at $\delta_c = 0$ and $\delta_c = 2\Delta_g$ as shown in Fig.6.(a).

Figure 5.(e) shows the result for the case of $\epsilon = -\frac{\pi}{6}$ which shows that there are three transmission peaks and no switching occurs at any two photon resonance condition. The symmetric result of the 13-level system is not reproduced in the case of the 16-level system. The reason for the absence of absorption for $\epsilon = -\frac{\pi}{6}$ in which the condition $\Omega_c^- > \Omega_c^+$ ($\Omega_p^- < \Omega_p^+$) is maintained is due to the involvement of the Zeeman state $|10\rangle$. The weak σ^- component of the probe, which was responsible for the absorption in the 13-level system, is now red detuned with respect to $|3\rangle \rightarrow |14\rangle$ and blue detuned with respect to $|3\rangle \rightarrow |10\rangle$. This kind of scenario leads to increased scattering of probe through both the states $|10\rangle$ and $|14\rangle$

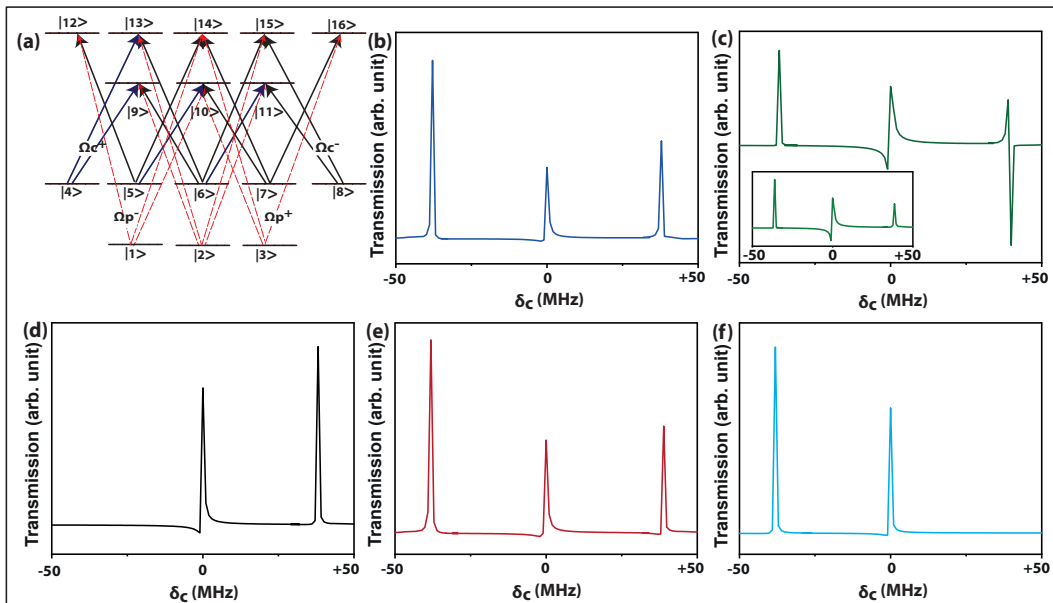


FIG. 5. (a) The energy level diagram showing 16 levels which are the zeeman sublevels (shown without the splitting). The red (dashed) line represents the weak probe and the black (solid) line is used to represent the strong probe. Numerical results showing transmission of the weak probe as a function of pump detuning (δ_c) at fixed value of $B=30\text{G}$, probe intensity = 0.3 mW/cm^2 and pump intensity = 161.2 mW/cm^2 : (b). three transmission peaks for ellipticity (ϵ) = 0° , (c). two transmission and one absorption (at blue detuned part) for $\epsilon = +30^\circ$. Inset shows that three transmission is possible if the coherence terms $\bar{\rho}_{1,10}$ and $\bar{\rho}_{1,14}$ are excluded from the calculations (Eq.15), (d). two transmission peaks for $\epsilon = +45^\circ$, (e). three transmission peaks for $\epsilon = -30^\circ$, and (f). two transmission peaks for $\epsilon = -45^\circ$.

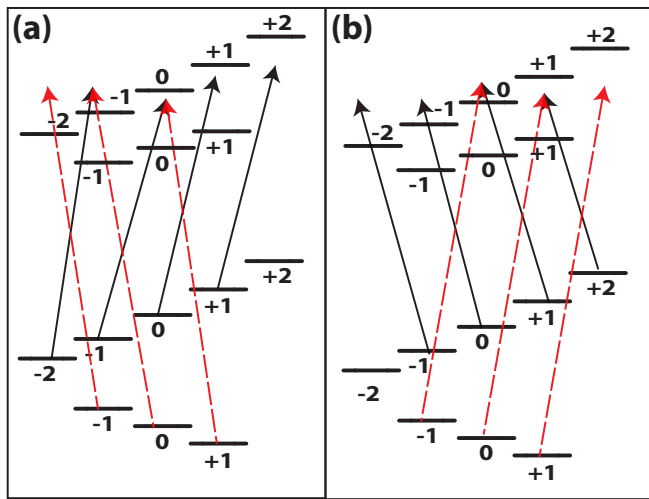


FIG. 6. Energy level diagrams for 16-level systems showing Λ systems each in case of (a). $\epsilon = +45^\circ$ and (b). $\epsilon = -45^\circ$

as both levels are taken to be within the Doppler width (Δ_D) in the system, i.e., $\Delta_D > \omega_{14} - \omega_{10}$. In other words, the probe is far detuned to the level $|14\rangle$ while at the same time being near detuned to the state $|10\rangle$. This condition leads to the reduction in cross-section (σ_{TPA}) of the two photon absorption phenomena as

$\sigma_{\text{TPA}} \propto \delta_p$ [42]. For $\epsilon = \frac{\pi}{6}$, on the other hand, the weak σ^+ component of the probe is blue detuned with respect to both the transitions $|1\rangle \rightarrow |10\rangle$ and $|1\rangle \rightarrow |14\rangle$. This increases the probability of a two-photon absorption process as the probe becomes far detuned with respect to both the states $|10\rangle$ and $|14\rangle$.

For $\epsilon = \frac{-\pi}{4}$, similar to a 13-level system, two transmission peaks occur at $\delta_c = -2\Delta_g$ and $\delta_c = 0$ (Fig.5(f)). Four Λ systems are present at this polarisation of light fields where Ω_p^- and Ω_c^- components are absent (Fig.6(b)).

IV. EXISTENCE OF STEADY STATE SOLUTIONS.

While writing the total Hamiltonian(H), we assumed that the system has a time and phase independent basis (co-rotating frame) which ensured the existence of a steady state solution. A general condition for this existence of the steady state solution is presented in this section. Let us take a case of N number of energy levels in a cascade system as shown in Fig.7. There are in total N fields with Rabi frequency $\Omega_1, \Omega_2, \dots, \Omega_N$ stimulating N transitions. The interaction Hamiltonian in

Schrodinger's picture for this $N \times N$ system is,

$$\bar{H}_I = -\frac{\hbar}{2} \left(\sum_{j=1}^{N-1} \Omega_j e^{i\beta_j} |j\rangle \langle j+1| + \sum_{j=1}^{N-1} \Omega_j^* e^{-i\beta_j} |j+1\rangle \langle j| + \Omega_N e^{i\beta_N} |1\rangle \langle 3| + \Omega_N^* e^{-i\beta_N} |3\rangle \langle 1| \right) \quad (16)$$

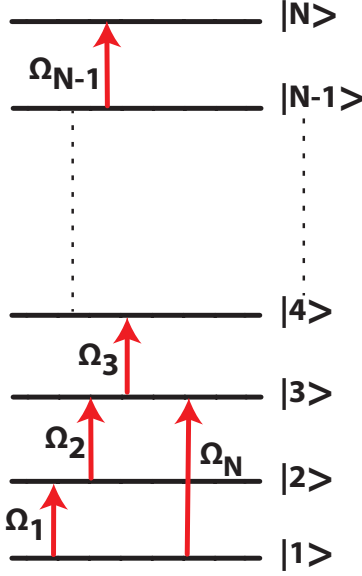


FIG. 7. N energy levels connected by N different frequency components of light field having a Rabi-frequency Ω_j and with arbitrary phases. For N energy levels N connections would mean one of the level must be connected twice (Ω_N). If there is only $N-1$ frequency components, phase and time independent basis exist for the system and no multiphoton resonance and phase matching is required for the system to have a steady state solution.

Where, Ω_j is the Rabi frequency of the transition $|j\rangle \rightarrow |j+1\rangle$ and $\beta_j = \omega_j t + \phi_j$ is the phase of the fields. We look for a unitary matrix $U = \sum_{k=1}^N e^{i\alpha_k} |k\rangle \langle k|$ such that $U\bar{H}_I U^\dagger$ becomes time and phase independent.

$$H_I = U\bar{H}_I U^\dagger = -\frac{\hbar}{2} \left(\sum_{k=1}^N e^{i\alpha_k} |k\rangle \langle k| + \sum_{j=1}^{N-1} \Omega_j e^{i\beta_j} |j\rangle \langle j+1| + \sum_{j=1}^{N-1} \Omega_j^* e^{-i\beta_j} |j+1\rangle \langle j| + \Omega_N e^{i\beta_N} |1\rangle \langle 3| + \Omega_N^* e^{-i\beta_N} |3\rangle \langle 1| + \sum_{l=1}^N e^{-i\alpha_l} |l\rangle \langle l| \right) \quad (17)$$

The problem then reduces to the following set of N linear equations,

$$\beta_k + \alpha_k - \alpha_{k+1} = 0 \quad k = 1, 2, \dots, N-1 \quad (18)$$

$$\beta_N + \alpha_1 - \alpha_3 = 0 \quad (19)$$

A non-trivial solution for these N linear equations can be found by taking $\alpha_1 = 0$ which gives for $N > 1$,

$$\alpha_N = \sum_{i=2}^N \beta_{i-1} \quad \text{with} \quad \beta_N = \beta_1 + \beta_2 \quad (20)$$

The condition $\beta_N = \beta_1 + \beta_2$ defines the so called multiphoton resonance ($\Omega_N = \omega_1 + \omega_2$) and phase matching ($\phi_N = \phi_1 + \phi_2$). Hence, for the existence of a time and phase independent basis for N fields with N energy levels multiphoton resonance and phase matching conditions needs to be satisfied. This is also true for a case where the number of fields is larger than the number of available states, which would add more conditions. On the other hand, if there was only $N-1$ fields with N energy levels no extra condition is needed for the existence of the co-rotating frame. This is a very handy result where only by counting the number of field components and available energy states, we can tell about the existence of the steady state solution for the problem.

A. Assumption and limitation of the model

In our model, for the case of a lin⊥lin fields i.e., $\epsilon = 0$ the total number of active transitions is 14 and 23 for a 13-level and 16-level system, respectively. This would mean that the system may not have steady-state solutions for arbitrary phases of the light fields. However, in an experiment, either one of the light fields is in scanning mode (frequency changes in time). For this case of scanning field if the condition $\tau_{coh} \cdot v_s < \Delta_g$ is satisfied, we assume that this reduces the number of active field components at a given time. v_s is the scan speed, τ_{coh} is the ground state coherence life time, and $\Delta_g = \frac{\mu_B B}{2\hbar}$ is the Larmor's frequency associated with the ground state electrons. Under this condition, no multi-photon resonance or phase matching between the light fields is required for the existence of a steady state. Hence, we assume that the form of the H_I can be written in a time- and phase-independent basis. The condition $\tau_{coh} \cdot v_s < \Delta_g$ also allows us to consider the system an open one where the re-population matrix is not needed for the steady state condition. Our model works for small values of magnetic field up to 30 G for the D_2 line. For larger values, the Zeeman states of other hyperfine states need to be considered to reproduce the experimental observations.

In the next section, we present an experiment performed in the D_2 line of ^{87}Rb at room temperature, where both the 13-level and 16-level results are observed but at two different values of magnetic field. The results for the 13-level system where only the Zeeman levels of $F' = 2$ are included match the experimental one at low magnetic fields. At higher values of the magnetic field, the experimental spectra started showing the features of a 16-level system. The amplitude and width of the two-photon res-

onance are not exactly confirmed with numerical results, which shows the limitations of our model. However, the nature and overall line shape of the experimental resonances are in good agreement with the numerical results.

V. EXPERIMENT ON D_2 LINE OF ^{87}Rb

A. Experimental setup

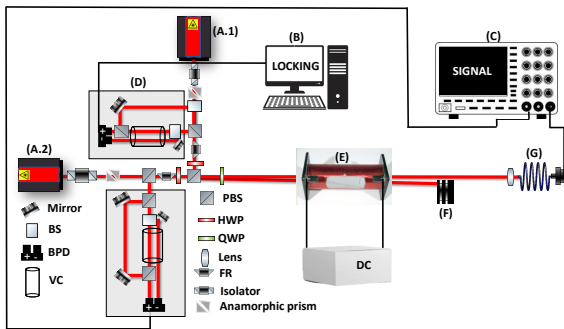


FIG. 8. Experimental setup used to obtain the experimental results. (A.1 and A.2) The laser sources. (B) Laser locking module. (C) Digital Oscilloscope. (D) Saturated absorption spectroscopy (SAS) setup. BS (Beam Splitter); BPD (Balanced Photo Detector); VC (Vapor Cell) (E) Solenoid with the vapor cell. The strength of the magnetic field is controlled using an external DC power supply. (F) Beam dump (G) Ultra fast photo detector.

The optical setup shown in Fig.8 was used for obtaining the experimental results. Both the laser sources (probe and pump) are generated from external feedback diode lasers with central wavelength of 780 nm having linewidth of 1 MHz. The experiments were performed in the D_2 line of ^{87}Rb atoms. Using the laser locking electronics (Topica digilock 110), the probe laser was locked from $F=1$ to $F'=2$ transition and the frequency of the pump laser was scanned across the hyperfine transitions. To avoid any back reflection optical isolators were used. The beam profile was also made nearly circular using anamorphic prism pair. The beam diameter of both the lasers are 0.2 cm. The signals produced with saturated absorption spectroscopy (SAS) was used as a frequency reference scale for both the lasers. Both the lasers were also passed through a faraday rotator for pre control of the polarisation before it is combined with a polarizing beam splitter (PBS). The power of both the lasers were controlled using a combination of half wave plate (HWP) and PBS. The ellipticity of both the laser is simultaneously tuned using a quarter wave plate (QWP). This technique helps in maintaining the orthogonal polarisation of both the laser fields while tuning the ellipticity. The experimental cell is a Rb vapor cell having dimension of 25 x 75 mm. It was maintained at room temperature with a temper-

ature controller system. A solenoid, with a length of 10 cm and a diameter of 6 cm, is wound with a Standard Wire Gauge (SWG) of 16 is used for generating the magnetic field. It consists of 590 turns and was subjected to an applied current between 0-1.5 A. The entire chamber enclosed with μ metal sheets to nullify the earth's magnetic field. The detected signal is measured using an fiber coupled ultra-fast photo detector and observed in a 5 channel oscilloscope.

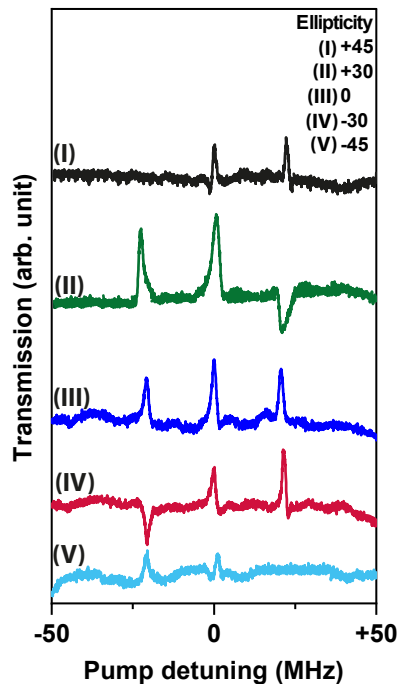


FIG. 9. Experimental results showing the transmission of the weak probe as a function of pump detuning at fixed value of $B= 17\text{G}$, probe intensity = 3.3 mW/cm^2 and pump intensity= 161.2 mW/cm^2 . Blue spectra (curve-III) is the result with ellipticity (ϵ)= 0^0 , three transmission peaks are observed. Green spectra and red spectra (curve-II and IV) are the results obtained for $\epsilon=\pm 30^0$, two transmission and one absorption peak is observed. Black and blue curve (curve-I and V) are the results obtained for $\epsilon=\pm 45^0$, two transmission peaks are observed.

B. Results

In the experiment, the probe is locked at the $|F=1\rangle \rightarrow |F'=2\rangle$ transition, and the pump is scanned around $|F=2\rangle \rightarrow |F'=2\rangle$. The probe and pump intensity are kept fixed at 3.3 mW/cm^2 and 161.2 mW/cm^2 throughout the study. The experimental results obtained for a magnetic field of 17 G are shown in Fig. 9. As discussed in the previous section, the ellipticity (ϵ) of both beams is simultaneously varied using a quarter wave plate. For the case when $\epsilon = 0$, three transmission peaks are observed (curve-III). The peak positions of the three peaks

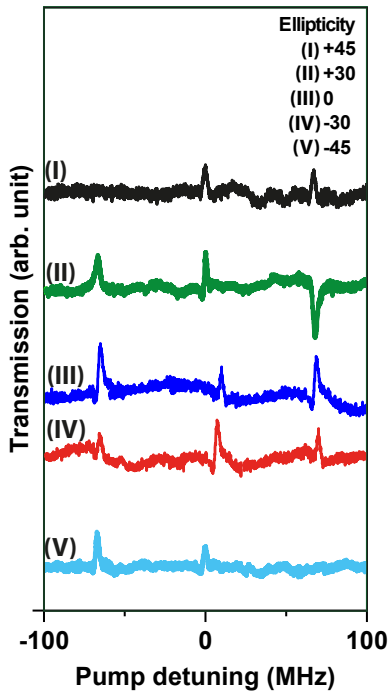


FIG. 10. Experimental results showing the transmission of the weak probe as a function of pump detuning at fixed value of $B=45\text{G}$, probe intensity = 3.3 mW/cm^2 and pump intensity = 161.2 mW/cm^2 . Blue spectra (curve-III) is the result with ellipticity (ϵ) = 0° , three transmission peaks are observed. Green spectra (curve-II) is the results obtained $\epsilon = +30^\circ$, two transmission and one absorption peak is observed. Red spectra (curve-IV) is the results obtained $\epsilon = -30^\circ$, three transmission peaks are observed. Black and blue curve (curve-I and V) are the results obtained $\epsilon = \pm 45^\circ$, two transmission peaks are observed.

are at $\delta_c = 0, \pm 2\Delta_g$ ($\Delta_g = \frac{\mu_B B}{2\hbar}$).

As discussed earlier, altogether, 10 Λ systems are responsible for these three transmission peaks. By tuning the ellipticity to $+30^\circ$ ($\epsilon = \frac{\pi}{6}$), one of the peaks ($+2\Delta_g$) converts to absorption (curve-II). By further changing the ellipticity to $+45^\circ$ ($\epsilon = \frac{\pi}{4}$), only two transmission peaks are observed (curve-I). For -30° ($\epsilon = -\frac{\pi}{6}$), the observation is similar to what is observed for $+30^\circ$. However, the position of the absorption peak is observed on the red detuned part of the spectrum (curve-IV). Observations similar to $+45^\circ$ are made when the ellipticity is tuned to -45° (curve-V). In this case too, the only difference is in the position of the two peaks. For ellipticity higher than 45° , the features repeated themselves, maintaining the symmetry we had observed for positive and negative values of ellipticity. The results are in complete agreement with the numerical results of the 13-level system. This shows that the effect of Zeeman states of $|F' = 1\rangle$ is negligible at this value of magnetic field for the D_2 line. We conclude that the transmission spectra of D_1 and D_2 lines of ^{87}Rb

would be the same at low values of magnetic field.

The experimental observations for a magnetic field of 45 G are shown in Fig.10. The reason for increasing the magnetic field was to create a situation where the effects of other hyperfine levels became more prominent. For $\epsilon=0$, three transmission peaks are observed similar to what is observed for low magnetic field (curve-I). However, the amplitudes of these three peaks are different. For ellipticity equal to $+30^\circ$, an absorption peak on the blue detuned part and two transmission peaks are observed, as shown in curve-II of Fig.10. Two transmission peaks are visible for both the case of circularly polarised light fields, i.e., for $+45^\circ$ and -45° as shown in Fig.10 (curve-I and V respectively). The main difference in the observations for this case as compared to the low magnetic field is the absence of symmetry with respect to the sign of ellipticity. The results produced here for $B=45\text{ G}$ are in agreement with the 16-level model system. Hence, we conclude that for our model system of D_2 line of ^{87}Rb at higher magnetic field, nearby Zeeman states of $F' = 1$ actively participate in two-photon processes.

VI. CONCLUSION

In conclusion, our numerical work focused on a large Zeeman manifold within an electromagnetically induced transparency (EIT) medium, using the D_1 and D_2 lines of ^{87}Rb as a model system. We investigated two different models comprising 13 and 16 energy levels, respectively, in the context of pump-probe spectroscopy with varying polarization's of the light fields. By applying a longitudinal magnetic field and manipulating the ellipticity of the light fields while maintaining orthogonal polarization's, we made several key observations. For the 13-level system, at a specific ellipticity value of $\epsilon = +30^\circ$, our results demonstrated the coexistence of EIT and two-photon absorption in the probe spectra. Notably, the position of the two-photon absorption peak shifted from the blue-detuned region to the red-detuned region, and vice versa, upon flipping the sign of the ellipticity. This intriguing symmetry was absent in the 16 level system, where two photon absorption only occurred at positive ellipticity values. We attributed this behavior to the optical anisotropy arising from the unequal population distribution in the ground Zeeman levels due to the change in ellipticity. Our findings emphasized that the presence of a longitudinal magnetic field and the modulation of light polarization ellipticity induce optical anisotropy, resulting in the absorption of a weak probe. We highlighted that for a large number of interacting states and various field components, the existence of a steady state crucially depends on multi-photon resonance and phase matching conditions. However, in our model, we did not require these conditions, suggesting a departure from the typical

assumptions in similar systems. Furthermore, to validate our numerical results, we conducted experiments at two distinct magnetic field strengths in the D₂ line of ⁸⁷Rb. The experimental spectra closely matched our numerical predictions, confirming the need for a 16-level (or higher) system to accurately represent the response of the D₂ lines of ⁸⁷Rb at larger magnetic field values. We conclude that, for magnetic fields up to 20 G, both the D₁ and D₂ lines of ⁸⁷Rb exhibits identical spectra, effectively described by the 13-level model. Finally we discussed the assumptions and limitations of our model acknowledging its simplifications and potential deviations from experimental results. In summary, our study sheds light on the intricate interplay between Zeeman sublevels, mag-

netic fields, and light polarization in EIT systems. The observed phenomena provide valuable insights for designing and optimizing magnetic field direction-dependent optical switching, where the magnetic field direction can be used as a knob to switch between subluminal and superluminal resonances [43, 44]. This work can also contribute in improving the sensitivity of EIT-based magnetometers [38] by controlling the influence of nearby hyperfine states. Additionally, our work has potential applications in the field of optical quantum gates [45]. Further investigations considering additional energy levels and exploring various experimental conditions would be beneficial for a comprehensive understanding of these complex systems.

-
- [1] Z.-Y. J. Ou, *Multi-photon quantum interference*, Vol. 43 (Springer, 2007).
- [2] M. Fleischhauer, A. Imamoglu, and J. P. Marangos, Electromagnetically induced transparency: Optics in coherent media, *Reviews of modern physics* **77**, 633 (2005).
- [3] K.-J. Boller, A. Imamoglu, and S. E. Harris, Observation of electromagnetically induced transparency, *Physical Review Letters* **66**, 2593 (1991).
- [4] S. E. Harris, J. Field, and A. Imamoglu, Nonlinear optical processes using electromagnetically induced transparency, *Physical Review Letters* **64**, 1107 (1990).
- [5] A. Lezama, S. Barreiro, and A. Akulshin, Electromagnetically induced absorption, *Physical Review A* **59**, 4732 (1999).
- [6] A. Taichenachev, A. Tumaikin, and V. Yudin, Electromagnetically induced absorption in a four-state system, *Physical Review A* **61**, 011802 (1999).
- [7] B. Dalton, R. McDuff, and P. Knight, Coherent population trapping, *Optica Acta: International Journal of Optics* **32**, 61 (1985).
- [8] E. Arimondo, V coherent population trapping in laser spectroscopy, in *Progress in optics*, Vol. 35 (Elsevier, 1996) pp. 257–354.
- [9] R. Willis, F. Becerra, L. Orozco, and S. Rolston, Four-wave mixing in the diamond configuration in an atomic vapor, *Physical Review A* **79**, 033814 (2009).
- [10] C. McCormick, V. Boyer, E. Arimondo, and P. Lett, Strong relative intensity squeezing by four-wave mixing in rubidium vapor, *Optics letters* **32**, 178 (2007).
- [11] Y. Zhang, U. Khadka, B. Anderson, and M. Xiao, Temporal and spatial interference between four-wave mixing and six-wave mixing channels, *Physical review letters* **102**, 013601 (2009).
- [12] H. Kang, G. Hernandez, and Y. Zhu, Slow-light six-wave mixing at low light intensities, *Physical review letters* **93**, 073601 (2004).
- [13] Y. Zhang, A. W. Brown, and M. Xiao, Opening four-wave mixing and six-wave mixing channels via dual electromagnetically induced transparency windows, *Physical review letters* **99**, 123603 (2007).
- [14] J. Bjorkholm and P. Liao, Line shape and strength of two-photon absorption in an atomic vapor with a resonant or nearly resonant intermediate state, *Physical Review A* **14**, 751 (1976).
- [15] S. Hendrickson, M. Lai, T. Pittman, and J. Franson, Observation of two-photon absorption at low power levels using tapered optical fibers in rubidium vapor, *Physical review letters* **105**, 173602 (2010).
- [16] A. J. Olson and S. K. Mayer, Electromagnetically induced transparency in rubidium, *American Journal of Physics* **77**, 116 (2009).
- [17] D. Höckel and O. Benson, Electromagnetically induced transparency in cesium vapor with probe pulses on the single-photon level, *Physical review letters* **105**, 153605 (2010).
- [18] S. Balushev, N. Leinfellner, E. Korsunsky, and L. Windholz, Electromagnetically induced transparency in a sodium vapour cell, *The European Physical Journal D-Atomic, Molecular, Optical and Plasma Physics* **2**, 5 (1998).
- [19] A. Sargsyan, P. Petrov, T. Vartanyan, and D. Sarkisyan, Electromagnetically induced transparency in potassium vapors: features and restrictions, *Optics and Spectroscopy* **120**, 339 (2016).
- [20] V. M. Acosta, K. Jensen, C. Santori, D. Budker, and R. G. Beausoleil, Electromagnetically induced transparency in a diamond spin ensemble enables all-optical electromagnetic field sensing, *Physical review letters* **110**, 213605 (2013).
- [21] R. K. Singh, N. Sharma, I. H. Subba, S. Chatterjee, and A. Tripathi, Light shift induced modification of electromagnetically induced resonances in atomic vapor, *Optics Communications* **537**, 129466 (2023).
- [22] S. R. Chanu, K. Pandey, and V. Natarajan, Conversion between electromagnetically induced transparency and absorption in a three-level lambda system, *Europhysics Letters* **98**, 44009 (2012).
- [23] A. Huss, E. Korsunsky, and L. Windholz, Phase control of electromagnetically induced transparency in a double-lambda system, *Journal of Modern Optics* **49**, 141 (2002).
- [24] X. Xu, S. Shen, and Y. Xiao, Tuning the phase sensitivity of a double-lambda system with a static magnetic field, *Optics Express* **21**, 11705 (2013).
- [25] C. Goren, A. Wilson-Gordon, M. Rosenbluh, and H. Friedmann, Sub-doppler and subnatural narrowing of an absorption line induced by interacting dark resonances in a tripod system, *Physical Review A* **69**, 063802 (2004).

- [26] N. Ram, M. Pattabiraman, and C. Vijayan, Effect of ellipticity on hanle electromagnetically induced absorption and transparency resonances with longitudinal and transverse magnetic fields, *Physical Review A* **82**, 033417 (2010).
- [27] D. V. Brazhnikov, A. V. Taichenachev, and V. I. Yudin, Polarization method for controlling a sign of electromagnetically-induced transparency/absorption resonances, *The European Physical Journal D* **63**, 315 (2011).
- [28] M. Bhattarai, V. Bharti, and V. Natarajan, Tuning of the hanle effect from eit to eia using spatially separated probe and control beams, *Scientific Reports* **8**, 7525 (2018).
- [29] N. Ram and M. Pattabiraman, Sign reversal of hanle electromagnetically induced absorption with orthogonal circularly polarized optical fields, *Journal of Physics B: Atomic, Molecular and Optical Physics* **43**, 245503 (2010).
- [30] R. K. Singh, N. Sharma, I. H. Subba, S. Chatterjee, and A. Tripathi, Competition between off-resonant and on-resonant processes in electromagnetically induced transparency in presence of magnetic field, *Physics Letters A* **416**, 127673 (2021).
- [31] M. Bhattarai, V. Bharti, V. Natarajan, A. Sargsyan, and D. Sarkisyan, Study of eit resonances in an anti-relaxation coated rb vapor cell, *Physics Letters A* **383**, 91 (2019).
- [32] B. C. Das, A. Das, D. Bhattacharyya, and S. De, Effects of vector magnetic field on electromagnetically induced transparency with lin perp. lin polarization, *JOSA B* **38**, 584 (2021).
- [33] V. S. Chauhan, R. Kumar, D. Manchaiah, and R. K. Easwaran, Enhancement of electromagnetically induced transparency and absorption signals in 85 rb atomic vapor medium by using a small external magnetic field, *JOSA B* **38**, 630 (2021).
- [34] A. Sargsyan, R. Mirzoyan, and D. Sarkisyan, Splitting of the electromagnetically induced transparency resonance on 85 rb atoms in strong magnetic fields up to the paschen-back regime, *JETP letters* **96**, 303 (2012).
- [35] S. Iftiqar and V. Natarajan, Line narrowing of electromagnetically induced transparency in rb with a longitudinal magnetic field, *Physical Review A* **79**, 013808 (2009).
- [36] C. Mishra, A. Chakraborty, A. Srivastava, S. Tiwari, S. Ram, V. Tiwari, and S. Mishra, Electromagnetically induced transparency in λ -systems of 87 rb atom in magnetic field, *Journal of Modern Optics* **65**, 2269 (2018).
- [37] S. Bhushan, V. S. Chauhan, M. Dixith, and R. K. Easwaran, Effect of magnetic field on a multi window ladder type electromagnetically induced transparency with 87rb atoms in vapour cell, *Physics Letters A* **383**, 125885 (2019).
- [38] V. Yudin, A. Taichenachev, Y. Dudin, V. Velichansky, A. Zibrov, and S. Zibrov, Vector magnetometry based on electromagnetically induced transparency in linearly polarized light, *Physical Review A* **82**, 033807 (2010).
- [39] L. Ma, D. Anderson, and G. Raithel, Paschen-back effects and rydberg-state diamagnetism in vapor-cell electromagnetically induced transparency, *Physical Review A* **95**, 061804 (2017).
- [40] D. A. Steck, Rubidium 87 d line data, (2001).
- [41] I. H. Subba, R. K. Singh, N. Sharma, S. Chatterjee, and A. Tripathi, Understanding asymmetry in electromagnetically induced transparency for 87 rb in strong transverse magnetic field, *The European Physical Journal D* **74**, 1 (2020).
- [42] R. Finkelstein, S. Bali, O. Firstenberg, and I. Novikova, A practical guide to electromagnetically induced transparency in atomic vapor, *New Journal of Physics* **25**, 035001 (2023).
- [43] H. M. Dong, T. D. Thanh, N. T. T. Hien, L. T. Y. Nga, and N. H. Bang, Controlling optical switching by an external magnetic field in a degenerate vee-type atomic medium, *Physics Letters A* **469**, 128765 (2023).
- [44] G. Agarwal, T. N. Dey, and S. Menon, Knob for changing light propagation from subluminal to superluminal, *Physical Review A* **64**, 053809 (2001).
- [45] C. Ottaviani, S. Rebić, D. Vitali, and P. Tombesi, Quantum phase-gate operation based on nonlinear optics: Full quantum analysis, *Physical Review A* **73**, 010301 (2006).